


Article

Assessment of Mutual Variation of Near-Surface Air Temperature, Land Surface Temperature and Driving Urban Parameters at Urban Microscale

Deniz Gerçek ^{1,*}  and İsmail Talih Güven ²¹ Department of City and Regional Planning, Izmir Institute of Technology, 35433 Izmir, Türkiye² Department of Geophysics Engineering, Kocaeli University, 41001 İzmit, Türkiye; talihguven@yahoo.com

* Correspondence: denizgercek@iyte.edu.tr

Abstract: The Urban Heat Island (UHI) effect is of critical concern for cities' adaptation to climate change. The UHI effect shows substantial intra-urban variation at the city microscale, causing disparities in thermal comfort and energy consumption. Therefore, air temperature assessment should be prioritized for effective heat mitigation and climate adaptation. However, meteorological stations' spatial distribution is far from meeting the scale that the UHI and its driving parameters operate. This limitation hampers demonstrating the intra-city variability of UHI and its origin of sources; for example, most studies employ Land Surface Temperature (LST), usually without demonstrating the relationship between UHI and LST. The current body of knowledge on urban climate implies a much better understanding and more detailed information on the spatial pattern of UHI and the driving factors to provide decision-makers with tools to develop effective UHI mitigation and adaptation strategies. In an attempt to address the adequacy of the use of LST and UPs in describing the intra-city variability of UHI, this study investigates the relationship between LST daytime and nighttime, and air temperature (Ta) daytime and nighttime, and driving urban parameters (UPs) of UHI together. Although it is well recognized that the intensity of the UHI is characterized by Ta, particularly at night, so-called nocturnal UHI, the use of remotely sensed LST is common, owing to the lack of spatially detailed Ta data in cities. Our findings showed that nocturnal UHI is weakly correlated with nighttime LST with a Pearson correlation (r) of 0.335 at $p > 0.05$ and that it is not correlated with daytime LST for the case study, highlighting the need for Ta observations for representing the intra-urban variation of nocturnal UHI. Among UPs, Sky View Factor (SVF), Building Volume Density (BVD), and Road Network Density (RND) explained 69% of the variability of Ta nighttime that characterizes nocturnal UHI. Therefore, UPs that performed well in estimating nocturnal UHI may be used in the absence of densely distributed Ta measurements. In a further investigation of the urban cooling phenomenon based on UHI diurnal changes, a particular region with high nighttime temperatures spoiled the Ta daytime and nighttime coherence. This region is characterized by high Mean Building Height (MBH), BFD, and BVD that re-emits heat, low SVF that prevents urban cooling, and high RND that releases extra heat at night. These particular UPs can be of prior interest for urban cooling. The present study, exploring the relationships of LST and Ta in a diurnal context, offers a further understanding of the preference of LST, Ta, or UPs to characterize UHI. Ta, in relation to major causative factors (UPs), provides insights into addressing the localities most vulnerable to the UHI effect and possible strategies targeting heat mitigation for sustainability and climate change resilience.

Keywords: Urban Heat Island (UHI); Land Surface Temperature (LST); near-surface air temperature (Ta); climate change



Citation: Gerçek, D.; Güven, İ.T. Assessment of Mutual Variation of Near-Surface Air Temperature, Land Surface Temperature and Driving Urban Parameters at Urban Microscale. *Sustainability* **2023**, *15*, 15710. <https://doi.org/10.3390/su152215710>

Academic Editor: Mohammad Aslam Khan Khalil

Received: 23 September 2023

Revised: 30 October 2023

Accepted: 31 October 2023

Published: 7 November 2023



Copyright: © 2023 by the authors. Licensee MDPI, Basel, Switzerland. This article is an open access article distributed under the terms and conditions of the Creative Commons Attribution (CC BY) license (<https://creativecommons.org/licenses/by/4.0/>).

1. Introduction

Cities are currently home to more than half of the world's population. The projections imply that urban dwellers will reach about 68% of the world population and are expected

to double in number in developing countries by 2050 [1]. Urbanization is a complex transformation process that converts rural areas into urban land, accompanied by increased human activities that drastically modify the urban thermal environment [2]. The far-reaching consequences of urbanization on climate and society are manifested in the Urban Heat Island (UHI) effect, also recognized as the most notable impact of humans on the earth's climate [3–5]. UHI has a significant negative impact on the environment, human health, and energy consumption. UHI has been reported to induce health issues and mortality in large to medium sized cities [6–8] as well as megacities. Its environmental impacts include reduced biodiversity [9], degraded air quality [10], and degraded water quality [11]. UHI, creating thermal discomfort, also leads to increased energy consumption for cooling and air conditioning [12–14]. Rising urbanization is one of the defining trends of the last century, which is anticipated to extend into the near future, leading settlements to become citified and current cities to become metro- and megacities [15]. Climate change, the major challenge of the era, triggering extreme temperatures and heat waves, intensifies the UHI effect in cities and exaggerates its adverse impacts [16,17]. Due to this combined effect of rapid urbanization and climate change, the UHI phenomenon has become a crucial concern in meeting the sustainability development goals, i.e., making cities more resilient to climate change.

UHI is an urban climate phenomenon that is defined as urban areas being warmer than the surrounding rural and natural areas [18]. One of the most noticeable differences caused by urbanization is that soil and vegetation cover is replaced with impermeable surfaces and volumes, i.e., concrete, asphalt, and various construction materials. The thermophysical properties of those materials, e.g., albedo, emissivity, thermal conductivity, and heat capacity [19], alter the heat energy balance that regulates the urban thermal environment. Urban geometry forming canyons causes the heat to be trapped [20]. As a result, the heat in urban areas is significantly higher than in the rural surroundings. Urbanization also introduces a large amount of anthropogenic heat stemming from, e.g., emissions, heating, and combustion, further aggravating the UHI intensity [21]. UHI intensity is the indicator of how severe the UHI effect is and is simply formulated as $\Delta T = T_u - T_r$, where T_u is the urban temperature, and T_r is the rural temperature [18]. Most cities today are small-sized cities of populations up to 500 thousand [1]. At this scale of cities, the temperature may be observed to be 2–4 °C higher in urban areas compared to the rural surroundings [14,22,23]. As the city grows, this difference is reported to be higher [24] and can reach up to 10–12 °C at nights following hot days under calm and clear weather conditions [25,26]. Besides urban areas being warmer than their surroundings, large differences in temperatures exist within the urban environment, causing disparities in thermal comfort and energy consumption. Intra-urban differences in surface temperature may be even larger than urban vs. rural land [27]. Therefore, the variation of UHI intensity cannot be reduced to a simple urban–rural gradient [23].

Currently, more and more emphasis is being placed on intra-urban heat island assessment, mainly targeting heat mitigation for sustainability and climate change resilience. However, prior to its assessment, the types of UHI that have different underlying mechanisms should be acknowledged. UHI is characterized by different layers and surfaces and is commonly classified as canopy layer heat island (CLHI), boundary layer heat island (BLHI), and surface urban heat island (SUHI). Oke distinguishes two layers in the urban atmosphere: the canopy layer (CL) and the boundary layer (BL) [28]. Microclimate is defined as climate conditions at a “microscale” on the earth's surface [29]. The urban microclimate is governed at the microscale that is extended from the building scale to the city scale and characterized by a community of buildings or a neighborhood [30,31]. UHI is a microscale concept, and it is regulated by the natural and artificial materials in the immediate surroundings composed of the urban roughness elements, mainly buildings [32]. There is also another type, a non-atmospheric UHI, called the surface UHI (SUHI), which is the thermal emissivity of urban surfaces showing spatial variations. In UHI assessment studies, BLHI is usually off-target as it relates to the urban area as a whole and a mesoscale

concept associated with regional climate. There are mainly two eligible lines of research to quantify UHI: (i) UHI of the canopy layer (CLHI), and (ii) SUHI [3,33]. The first approach targeting CLHI is characterized by air temperature, also called near-surface air temperature or ambient temperature [32]. It is the temperature at the lowest part of the atmosphere that extends upwards from the ground approximately to the trees and buildings height [34] and is observed at 1.5–2 m distance from the ground [3]. In the development of urban climate, near-surface air temperature (T_a) in the canopy layer shows the most obvious modification compared to the natural or rural lands where air temperatures are high in highly urbanized areas [34–36]. Hence, the term UHI, unless otherwise stated, refers to the T_a [37].

Owing to its direct impact on human health and energy consumption, T_a measurements are of prime importance to the study of urban climate. Impermeable surfaces that absorb heat do not cool down enough, the heat is re-emitted and trapped in built environments, which leads to warm temperatures extending towards the night hours. This is the primary reason why UHI demonstrates the maximum intensity 3–5 h after sunset, and the nighttime T_a is considered a key indicator of UHI [25]. Quantification of UHI in the canopy layer requires the direct measurement of T_a . However, complex urban environments with diverse land use, texture, and density result in large temperature variations across a city, which cannot be represented by a small number of meteorological stations [38,39]. In the absence of representative observations, densely distributed in-situ measurements from fixed or mobile stations can theoretically represent the context of micro- and local scales [23,32,40]. However, in practice, the quality, coverage, distribution of the measurements, and costs are of concern [41]. Nevertheless, in-situ and/or mobile measurements are quite common, especially the low-cost in-situ measurements that have recently received growing interest for UHI mapping [39,42,43].

Besides the UHI approach mainly owing to its shortfalls, SUHI was introduced. With the advancement of remote sensing technologies enabling synoptic view and continuous acquisition, SUHI was proposed in an attempt to represent UHI [37]. SUHI is typically characterized by Land Surface Temperatures (LST) derived from airborne or satellite thermal infrared imagery, which provides a uniform means of effective radiating temperature of the Earth's surface [44]. Although LST can demonstrate surface temperature at large coverages and relatively high spatial resolution, the acquisition is limited to clear sky conditions and subject to temporal resolution that is insufficient to monitor daily or hourly intervals important for nighttime or daytime UHI assessment [45]. While UHI in the canopy layer is characterized by direct measurement of air temperature, SUHI is derived indirectly from the conversion of upwelling thermal radiance of the surface to temperature [37,46]. Nonetheless, the idea of using LST as an indicator of UHI is mainly based on the premise that surface temperature modulates the air temperature of the lowest layers of the urban atmosphere [37], and there is reasonable agreement at matching scales [47]. Several studies that facilitate both air and surface temperatures have documented a good consistency between T_a and LST [48–51], while some others reported either weak consistency or lack thereof [52,53]. Studies investigating T_a and LST for both day and night have found a stronger correlation between nighttime T_a and nighttime LST rather than daytime versions [54–56]. As LST modulates the T_a , along with other variables such as wind, moisture, and turbulent mixing [5], the complex linkage between air and surface temperatures cannot be easily quantified [37]. This complexity is the main reason that discourages the estimation of UHI through LST [5].

The representativeness of the thermal conditions can only be ensured at the local to the microscale context of surface geometry, land cover, and anthropogenic heat release [57]. Given that UHI at the micro- to local scale operates at distances from 1 cm to 1 km and is usually considered at less than 100 m [58], the main concerns with LST and T_a are as follows:

- i LST, even if effective in capturing the spatial pattern of surface temperature [3], is not a direct measure of UHI. Moreover, the diurnal cycle of UHI and SUHI are substantially different [47].

- ii Ta, although it directly characterizes UHI, represents the heat in the close vicinity. Unless forming a very dense network that is expensive to install and maintain, in-situ measurements are insufficient to represent the spatial variability of the UHI. Although some studies employ spatial interpolation, it is typically inadequate [59], as the urban form, texture, and land use characteristics are not steady across the space [39]. Therefore, representing UHI with LST or coarsely distributed Ta measurements can lead to erroneous results in studies targeting heat mitigation and may particularly be misleading in health-related subjects [34,53].

Urban parameterizations promote a better understanding of the major causative factors, addressing urban effects, including UHI, and the development of appropriate mitigation strategies [60]. As drivers of UHI formation, urban features, e.g., geometry and land use characteristics, are well-documented to be closely related to UHI, and have been extensively studied for their influence on UHI formation as gathered in several reviews [36,46,61]. There is a great deal of studies that explore and relate urban features and SUHI [62–66], as data for both are more available and easier to obtain. A study was implemented in the same case area as the present study, using elementary methods to see whether LST and some urban parameters were related [67]. Urban features' relation with Ta is also explored, yet studies are relatively scarce [38,68,69]. There are very few studies that explore urban features' relation with UHI and SUHI in parallel [70,71].

Of all the modifications produced by the urbanization process, urban geometry, thermal properties with their effects on radiation and heat storage [20,72], and anthropogenic heat [21] are the key factors in UHI formation. These factors are quantified as various spatial data including albedo, solar insolation, sky view factor, vegetation index, imperviousness, building density, population density, and traffic density, to name a few. All these data are referred to as "urban parameters" (UPs) throughout this study. Research that investigates the role of UPs has mainly taken two approaches into consideration. First is the direct use of urban features presumed to contribute to UHI formation. The second approach is the use of a classification of urban areas into local climate zones (LCZ) [73], characterized by a particular combination of UPs. However, the LCZ scheme employs only a few urban features, e.g., land cover and building density for zonation. Furthermore, temperatures may differ substantially even within LCZs [74]. In practice, mitigation and urban planning require a UHI map of proper scale that reveals the actual variability of UHI rather than the local thermal conditions of different LCZ types that are subject to generalization [75]. Therefore, the direct use of urban features is considered to better represent the microscale variation in urban climate. Effective scale is another important issue to be explored for the spatial extent dependence of UPs on UHI formation [23].

State-of-the-art UHI studies have reached a vast number, mainly due to the significance of the issue owing to the two overarching trends, climate change (CC) and urbanization. Among these studies, especially with the advancement of medium- to high-resolution thermal remote sensing, empirical studies that use LST for the determination of the UHI effect have increased considerably. Although LST characterizes SUHI, its use as an indicator of UHI is fairly common. The daily cycle of UHI, where nocturnal temperatures are pivotal, is usually disregarded in studies investigating UHI formation. LST, even if related, is not a perfect indicator of UHI. Therefore, using LST as an indicator of UHI might be problematic and needs further investigation. Besides, studies that substitute LST for UHI and investigate UPs in relation to SUHI formation became predominant. However, mainly owing to the lack of densely distributed Ta measurements, studies that model Ta based on UPs at the microscale, which may be helpful to guide strategies and critical measures to be taken for climate-proof cities, are scarce. In this context, it is beneficial to explore UPs' influence on forming UHI and SUHI separately. However, exploring UHI at a fixed scale is not adequate. Acknowledging that air temperature is affected by the broader surroundings of a particular location [76], it is essential to determine the optimal scales of indicator variables of UHI, i.e., LST and UPs.

It is evident that the diurnal cycle of atmospheric UHI and SUHI are considerably different [47]. However, studies that compare daytime and nighttime Ta or LST for UHI and SUHI, respectively, are scarce. Comparing diurnal differences, particularly of UHI, can enhance our understanding of how urban cooling progresses and whether cooling is prevented in particular regions of urban environments.

Based on the overview above, exploring both UHI and SUHI, for both day and night in relation to UPS, is considered a gap in urban climate studies. This study, besides attempting to verify the well-documented UHI–SUHI–UPS relation, addresses issues that are not given much emphasis and intends to answer the following research questions in an attempt to better understand urban climate through an empirical study.

- i Is LST a very good indicator of UHI? (How are Ta and LST related?)
- ii How are Ta and LST related to UPS? What are the most influential UPS in forming UHI and SUHI?

Regarding the first two questions, is there an effective scale on which LST and UPS operate mutually with the UHI spatial variability?

- iii What are the changes in Ta and LST in the diurnal cycle? (How are UHI day–night and SUHI day–night related?)

2. Data and Materials

To address the research questions, this study employs air measurements from the field for daytime and nighttime that coincide with the visit time of the remote sensing satellites of medium resolution that are used to derive LST for day and night. A set of parameters that represent urban geometry, thermal properties, and anthropogenic effects of the case area were quantified as spatial data, so-called UPS. Following a flowchart of analyses (Figure 1), the relationships between Ta, LST, and UPS were explored using multivariate statistics and graphical outputs.

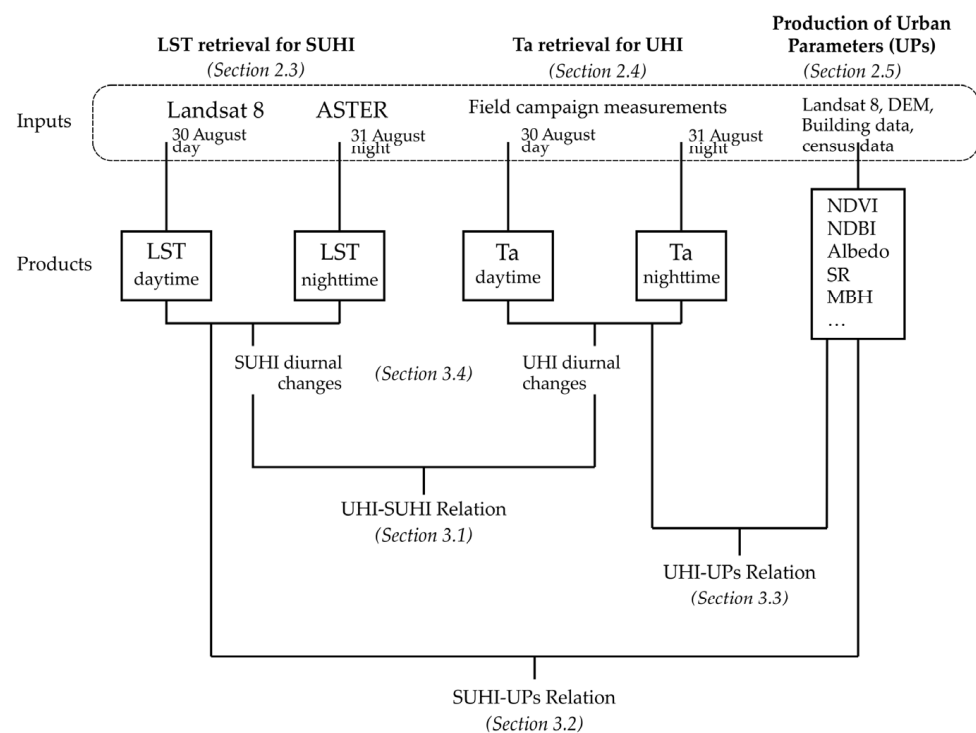


Figure 1. Flowchart of the study.

2.1. Case Study

A small-scale city (population < 500 thousand), which is the most common city type across the globe [1], that has about 350 thousand dwellers and an urbanization rate of 100%,

was selected as a case study. In arid to semi-arid climates, the UHI effect places more heat stress on organisms, including humans. Located in the Izmit Bay of the Marmara Sea in the northwest of Turkey (Figure 2), Izmit City has hot summers and mild winters, characterized by a transition between Csa and Cfa of the Köppen–Geiger climate classification [77]. The city has an average annual daily maximum temperature of 19.8 °C, where August is the hottest month with a long-time average of 30 °C. The city is in the hinterland of Istanbul and is the industrial heart of Turkey, with ports connected to major highways and railways. Due to the industrial activities and migration in the last several decades, Izmit has been subject to rapid urbanization that has produced many environmental challenges, including the Urban Heat Island effect.

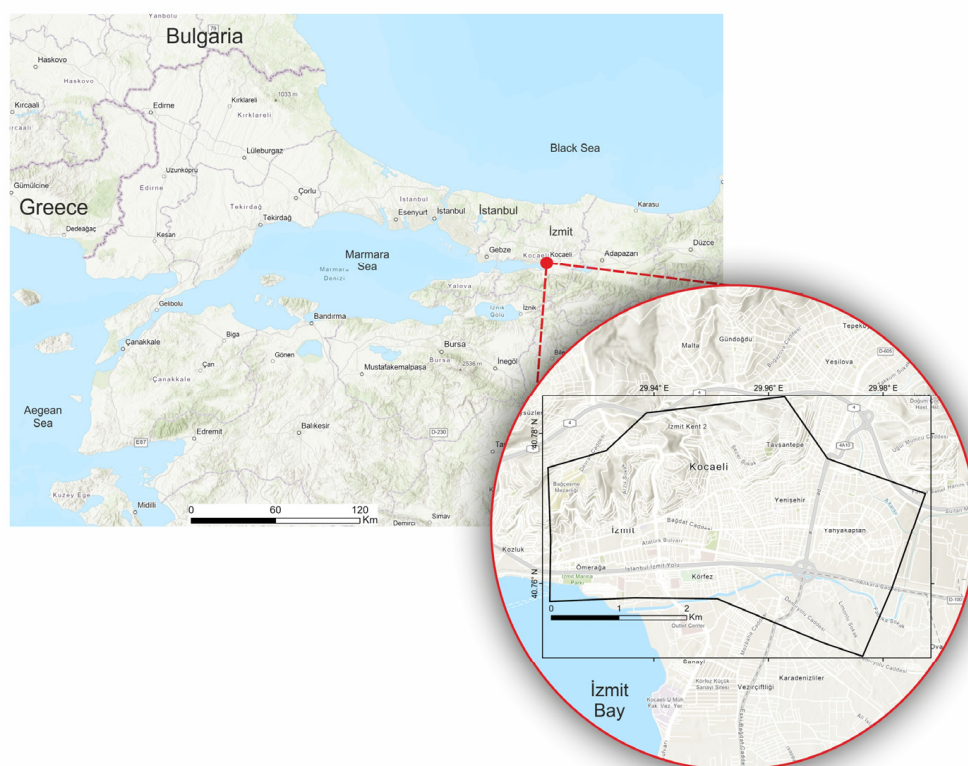


Figure 2. Study area.

The study area covers the city center with surrounding residential areas with the highest density of buildings and commercial facilities. The total area is about 14 km². The average elevation is 224 m, and the area is located on a plain with gently rising slopes towards the north of the study area.

2.2. Dataset

For the study, two successive medium-high resolution images to represent daytime and nighttime LST were acquired. August was selected as the image acquisition period, typically the hottest month of the city, and the acquisition dates were as follows:

Landsat 8 daytime images: 30 August 2015

ASTER nighttime images: 31 August 2015

LST products of high temporal resolution, e.g., MODIS that are freely available, usually suffer from low spatial resolution and are not adequate to represent intra-urban spatial variation of SUHI. ASTER thermal infrared imagery was purchased by funding, and the field campaigns we conducted in parallel with the same funding project in 2015. Therefore, the analyses in the study are based on a 2015 dataset.

The kinetic surface temperature product of ASTER that was gathered through a temperature emissivity separation method (TES) [78] was ready for use after geometric correction. The Landsat 8 thermal infrared bands had a spatial resolution of 100 m, and the ASTER surface temperature product had a spatial resolution of 90 m.

For T_a , mobile, low-cost in-situ observations were conducted for two successive periods (day and night) in parallel with the remote sensing image acquisition date/time. The field campaigns were organized on the same day of daytime image Landsat 8, and on the same night of the nighttime image (ASTER) to ensure that there was very little influence introduced by the weather conditions for comparisons. The field campaigns were implemented as follows:

Daytime campaign: the warmest time of the day between 14:00 and 15:00 on 30 August 2015.

Nighttime campaign: at midnight, 3.5 h after sunset (19:36), between 23:00 and 00:00 on 31 August 2015.

The (i) accuracy and (ii) distribution density of the measurements are of primary concern in T_a measurements [41].

- (i) In-situ measurements for UHI studies, either static or mobile, commonly employ instruments with an accuracy of $\pm 0.2\text{--}0.3\text{ }^\circ\text{C}$ [48,79–82] or $\pm 0.5\text{ }^\circ\text{C}$ [39,42,43,55,69], where low-cost instruments measuring at $\pm 0.5\text{ }^\circ\text{C}$ accuracy were reported to be effective in representing UHI and adequate in fine-scale spatiotemporal UHI mapping [42]. Two Kestrel-4500 weather meters were utilized for the air temperature observations for the study. The Kestrel weather meter is mounted with a hermetically sealed, thermally isolated precision thermistor with a fast response, marketed at a reasonable price, and easy to use and carry. It has a manufacturer-reported accuracy of $\pm 0.5\text{ }^\circ\text{C}$ at 1 sec response time and a resolution of $0.1\text{ }^\circ\text{C}$. Allowing meter readings to stabilize in a few minutes is suggested at each location to enhance reported accuracy [83,84].
- (ii) Studies for the local scales may utilize one measurement per 1 to 10 km^2 [69,75]. For microscales, this may be reduced to 1 measurement per 0.25 km^2 where there is approximately 300 to 600 m between measurement locations [23].

Intending to explore urban climate at the microscale, a number of 30 measurements was set for the study area of approximately 14 km^2 . The measurement locations were determined in the built-up land of the case area and then modified as some of the points were not accessible or did not represent critical localities. The sampling density is one measurement for less than 1 km^2 (approx. 0.7 km^2), and there is around 300 to 750 m between the points. The measurement points were spatially divided into two groups for the two instruments to complete the observations in a 1-h interval to minimize the temporal change of ambient temperature. The measurement points were accessed by car and then by walking. The instruments were placed on a tripod 1.75 m above the ground and at a distance of at least 2–3 m from buildings, roads, and heat-emitting sources. Daytime measurements were made in the shadow if possible, and a plastic shield over the instrument was used to prevent direct rays. The instrument logger was adjusted to automatically log every 10 s. At each location, 2–3 min were spent, where temperature records in the 1-min interval in the midst of each period were used for calculating T_a . Daytime and nighttime measurements were made at the same locations. Each campaign took about an hour to complete. A total of 28 points could be observed for the daytime temperatures. A total of 32 points for the nighttime temperatures was observed as there was less traffic and observers could visit more locations.

2.3. Land Surface Temperature (LST) Retrieval for SUHI

Of the two thermal datasets, the ASTER thermal product was ready for use after geometric correction. To calculate LST out of Landsat 8 thermal bands, the Radiative Transfer Equation (RTE) was employed as in recent studies [62,63,85] owing to its explicit method and straightforward application. Among two thermal bands of Landsat 8, band

10 was employed in the LST calculation. A four-phased transformation was carried out to reach surface kinetic temperature values from raw DN values of image cells.

- (i) DN values were converted to radiance using offset (bias) and gain values.
- (ii) Emissivity (ϵ) values were obtained using the Normalized Difference Vegetation Index (NDVI), which is closely related to emissivity [86] and used as thresholds to designate emissivity values as suggested by Sobrino [87].
- (iii) Atmospheric transmission (τ), downwelling atmospheric radiation (S_{\downarrow}), and upwelling atmospheric radiation (S_{\uparrow}) were derived using the Atmospheric Correction Parameter Calculator [88] that is based on MODTRAN Radiative Transfer code modeling from the National Centers for Environmental Prediction (NCEP) global atmospheric profiles database.
- (iv) The Radiative Transfer Equation (RTE), taking into account (ϵ), τ , S_{\downarrow} , and S_{\uparrow} as in Equation (1), is transformed by applying the inverse of the Plank as in Equation (2) to derive LST.

$$L_{\lambda}^{\circ} = [\epsilon B_{T_s} + 1(1 - \epsilon)S_{\downarrow}] \tau + S_{\uparrow} \quad (1)$$

where;

L_{λ} = Thermal radiance at sensor

B_{T_s} = blackbody radiance (Plank's law)

$$LST = \frac{C_2}{\lambda \ln \left\{ \frac{C_1}{\lambda^5 \left[\frac{L_{\lambda} - S_{\uparrow} - \tau(1 - \epsilon)S_{\downarrow}}{\tau \epsilon} \right]} \right\} + 1} \quad (2)$$

ϵ = Land surface emissivity

τ = Atmospheric transmissivity

S_{\uparrow} = Upwelling atmospheric radiance

S_{\downarrow} = Downwelling atmospheric radiance

λ = Effective band wavelength

Constants: $C_1 = 1.191 \times 10^8 \text{ W}\mu\text{m}^4\text{sr}^{-1} \text{ m}^{-2}$, $C_2 = 1.439 \times 10^4 \mu\text{m}\cdot\text{K}$

Finally, both ASTER and Landsat temperature values in Kelvin were converted to degrees Celsius ($^{\circ}\text{C}$) to acquire daytime LST and nighttime LST that represent the daytime and nighttime SUHI, respectively (Figure 3). Daytime and nighttime LST comparisons are essential for exploring LST diurnal changes and their relationship with the UHI formation.

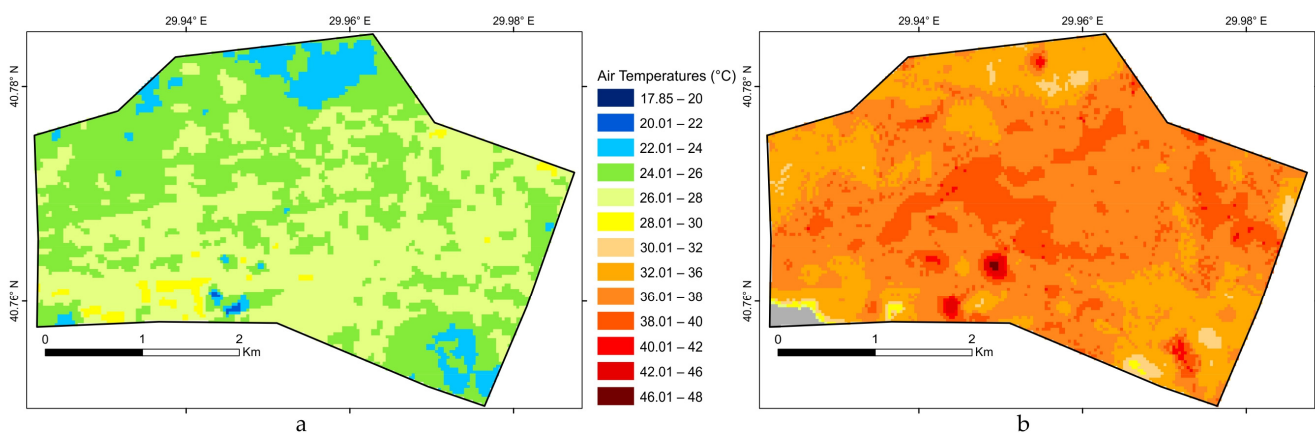


Figure 3. (a) LST nighttime (derived from ASTER); (b) LST daytime (derived from Landsat 8).

2.4. Air Temperature (T_a) Retrieval for UHI

Spatial variations in T_a can be captured via in-situ measurements that can accurately depict the target areas in small time and space scales [23]. A total of 28 points were observed for daytime and 32 points for nighttime at an accuracy of ± 0.5 °C and below.

Two of the observations were removed from the daytime set for fluctuated recordings, most possibly due to external heat sources, leaving 26 eligible observations for the daytime T_a (Figure 4).

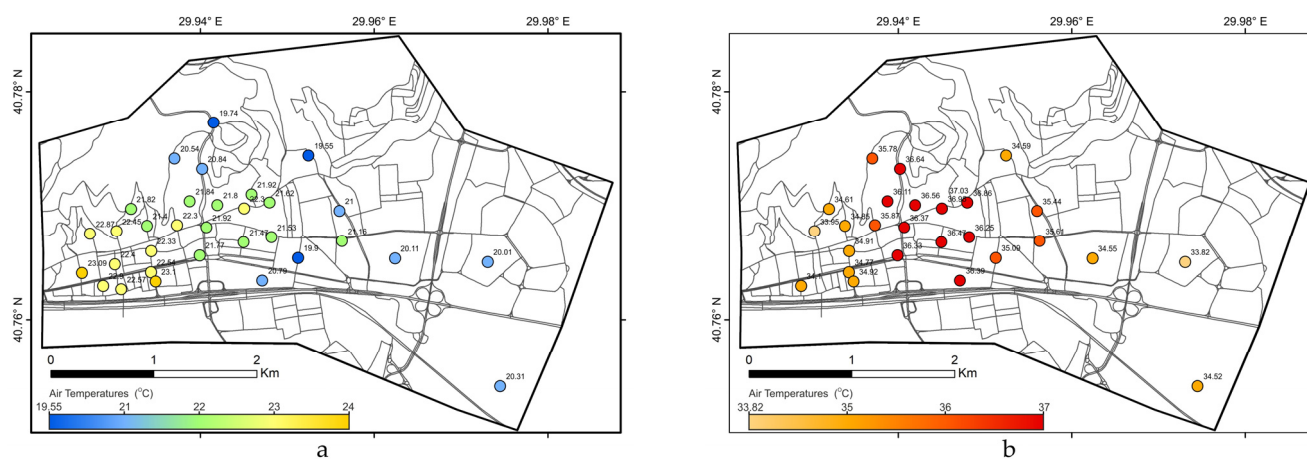


Figure 4. (a) T_a nighttime observations; (b) T_a daytime observations.

Although the measurements were complete in approximately one hour, considering that a temperature change had taken place, a time normalization that is common in UHI investigations was applied [23,75,89,90]. The T_a observation was adjusted to the mid-time based on fixed weather station measurements located in the city. Assuming that the time change rate is linear between the planned start and end times of the campaign, a unified time was defined as the mid-time, rather than the beginning or the end in an attempt to distribute possible errors more uniformly along the time span. Accordingly, for daytime observations, the unified reference time was set as 14:30, where the temperature difference between the beginning and the end (14:00, 15:00) is $+0.33$ °C. For nighttime observations, the unified reference time was set as 23:30, where the temperature difference between the beginning and the end (23:00, 00:00) is -1.2 °C. A temporal adjustment of 0 to max ± 0.16 and 0 to max ± 0.6 was made on the observed T_a values for daytime and nighttime observations, respectively.

2.5. Urban Parameters

Urban parameterizations are increasingly being used to promote a better understanding of urban climate and the major causative factors of UHI. In this study, we utilize key factors commonly employed, as summarized from numerous references. We broadly categorize those factors (UPs) based on their different sources as (i) biophysical, which relates to the thermal properties of the land use/land cover, (ii) morphometric, which relates to the urban form and geometry, and (iii) socioeconomic, that relates to urban density and functions that contribute to emissions.

There is a vast number of studies that use urban parameterizations and relate them to UHI or SUHI. Table 1 presents the UPs used in this study and their calculation method, along with the recent reference studies that utilize the same method. UPs and reference data used in calculating UPs in this study are depicted in Figure 5. UPs are essentially explored for their influence in forming UHI and SUHI, respectively.

Table 1. Urban Parameters (UPs) and their descriptions.

	Urban Parameters	Descriptions	References
Biophysical	Vegetation Index	$NDVI^a = \frac{(NIR-R)}{(NIR+R)}$ Normalized Difference Vegetation Index indicates the abundance of vegetation cover and is a major parameter that is commonly retrieved and used for UHI estimation.	[64,91–94]
	Built-up Index	$NDBI^a = \frac{(SWIR-NIR)}{(SWIR+NIR)}$ Normalized Difference Built-up Index indicates the fraction of built-up surfaces.	[94–96]
	Albedo	$Albedo^a = \frac{0.356\rho_2+0.130\rho_4+0.373\rho_5+0.085\rho_6+0.072\rho_7-0.0018}{0.356+0.130+0.373+0.085+0.072}$ Albedo, as formulated by Liang [97], was adopted. Albedo is the surface reflectance rate, where low albedo stores more energy and contributes to UHI.	[91,98]
	Solar Radiation	SR, incoming solar radiation (insolation), is the radiation energy received from the sun. Besides the day and time of the year, SR is determined by the topographic orientation (slope and aspect) of a surface. SR for the study was calculated based on the formulation by Fu and Rich [99], with slope and aspect derived from DEM ^b as input into the ArcGIS Area Solar Radiation tool.	[93]
Morphometric (urban)	Mean Building Height	$MBH^c = \text{height of buildings}/\text{number of buildings in the sample area}$ Building height is usually considered to reduce warming owing to the shade effect [64,82].	[38,64,82,95]
	Building Footprint Density	$BFD^c = \text{buildings footprint area}/\text{sample area}$ Division of the total building footprint by the site area. The density of the buildings in an area [14] indicates impermeable sealing that reduces evapotranspiration, hence cooling.	[46,63,64,82,95]
	Building Volume Density	$BVD^c = \text{Total volume of all buildings}/\text{sample area}$ Larger building blocks both release more longwave radiation and cause the heat to be trapped. The higher the building volume density, the larger its heat capacity [100].	[38,64]
	Sky View Factor	SVF is the ratio of visible sky from the ground to an unobstructed hemisphere [73]. A Digital Surface Model (DSM) was generated in ArcGIS by incorporating the building heights to the DEM ^b , which was then processed in the SVF tool of SAGA GIS [101].	[93,102,103]
Socio Economic	Population Density	$PD^d = \text{Number of people}/\text{sample area}$ Population density indicates the thermal load status of a city and is considered to influence urban climate [100,104].	[33,38,46,64]
	Road Network Density	$RND^e = \text{Kernel density of roads (road width weighted)}/\text{sample area}$ UHI is exacerbated by the anthropogenic heating from vehicles [44]. In the lack of traffic count data, road density was used as a proxy. A kernel density estimation tool was used to produce a road network density raster from the road length weighted by the road width.	[102]

^a NIR, R, and SWIR are the near-infrared, red, and mid-infrared bands of Landsat 8, respectively, and ρ represents Landsat 8 bands, ^b 1-m resolution Digital Elevation Model (DEM) was used. Building height data were rasterized and added to DEM to end up with a Digital Surface Model (DSM), ^c Building footprint and height data were obtained from the Municipality as vector data, ^d Number of people per building was calculated based on household census obtained from the Municipality, ^e Road data and related road widths were obtained from the Municipality.

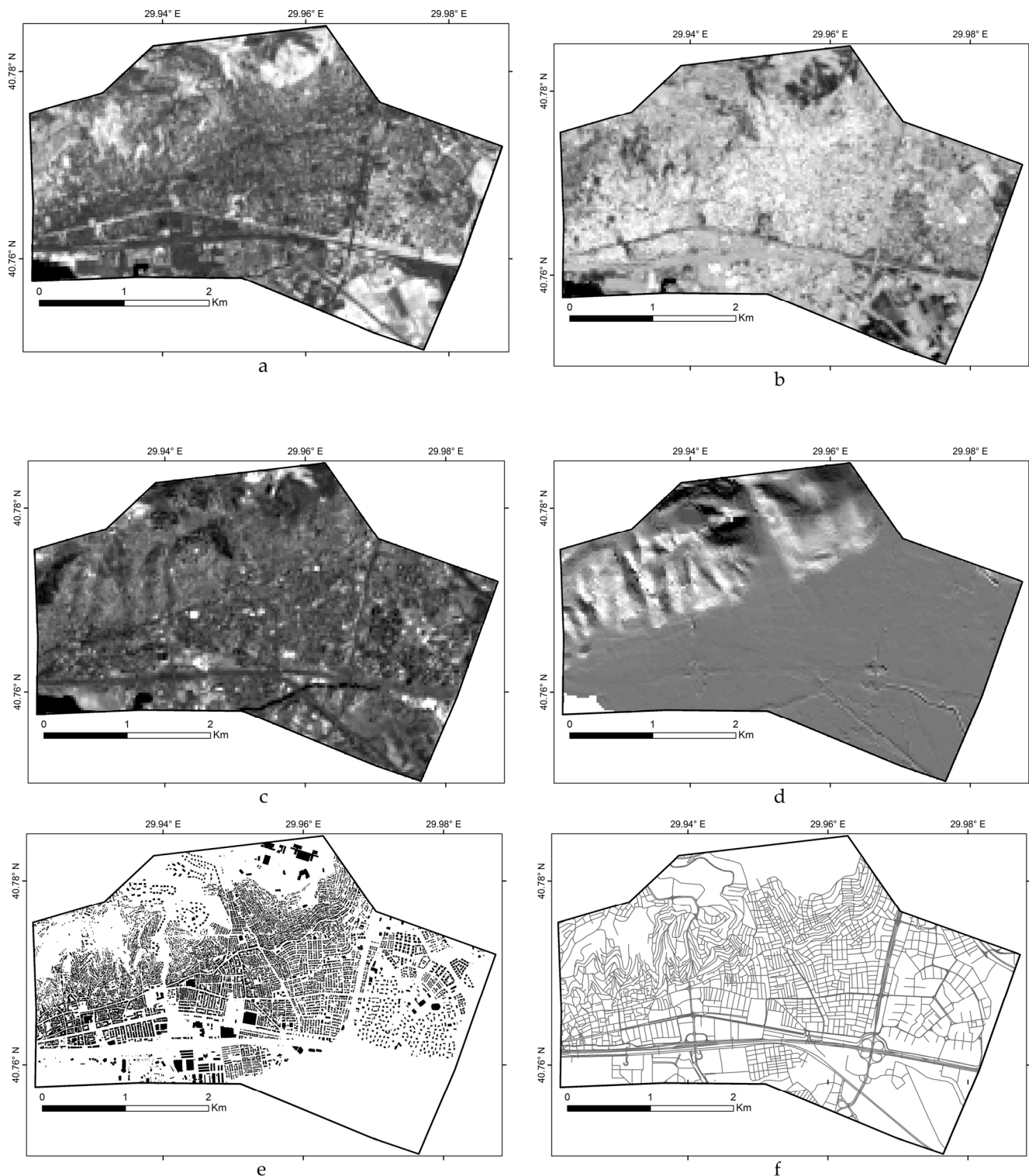


Figure 5. UPs and reference data for calculating UPs for the study. (a) NDVI, (b) NDBI, (c) Albedo, (d) SR, (e) Building data used in calculating MBH, BFD, and BVD. The PD. The SVF was calculated using a building height raster added to DEM, (f) Road data used in calculating RND.

2.6. Methods

This study aims to understand the urban climate by exploring the interrelationships between UHI, SUHI, and the UPs at the microscale using multivariate statistics and GIS tools. The associations between the indicators were explored through correlation analysis. The Pearson correlation, which measures the strength of a linear association between

two variables, was used. A correlation matrix was developed to examine the strength of bivariate relationships between Ta, LST, and UPs. LST and UPs were datasets with continuous coverage in raster format. All raster datasets of LST and UPs were resampled to a common resolution of 30 m for convenience. Ta points coincide only with one or a few pixels of the data, which would hardly produce reliable statistics. The correlation between air temperature at a point and land cover composition within a particular buffer area of that location is well documented [105]. Therefore, buffers of various sizes were produced that center Ta locations in order to make UHI data compatible with other datasets. The reason for utilizing varying sizes of buffers is to quantitatively assess the effective scale that the UHI phenomenon is associated with the UPs. In urban climate studies that use Ta measurements, fixed buffers of sizes as small as 10 m [106], 125 m [107], and 300 m [105] have been used. Some studies use a series of buffers, e.g., 20 to 300 m [23] and 50 to 1000 m [108], to determine critical buffer width, producing the highest correlation for the numerous explanatory variables they use. In the present study, we adopted buffer sizes at eight levels, starting from 25 m up to 200 m, as we have densely distributed observations to represent UHI at the microscale in a relatively small case area.

A multiple linear regression (MLR) using stepwise backward elimination was implemented to analyze the multivariate relationship between UHI, SUHI, and the driving UPs. A MLR is a model for predicting the value of a dependent variable based on multiple independent variables, where stepwise backward elimination starts with the complete list of independent variables and successively eliminates non-significant variables until reaching a reduced model with a high performance of estimating the dependent variable. In the present study, Land Use Regression (LUR), a specialized version of MLR for geospatial independent variables, was adopted. LUR is a prevalent method in public health studies, especially in modeling air pollution [109,110]. LUR also has found an application domain in urban climate studies [23,38,108]. LUR estimates the UHI in the study area by treating it as the response variable of a multiple linear regression model (MLR) of several explanatory variables: UPs for this case. LUR was implemented using the buffer size representing the most effective scale of UPs for LST and Ta. The mean zonal statistics for particular buffers where UPs have the highest correlation with LST or Ta were utilized for the estimation of those.

3. Results and Discussions

The LST and Ta measurements for both day and night and UPs were analyzed for their correlation. All datasets are of ratio scale, without significant outliers, and have shown linear patterns of match in dot plots that conform to a Pearson Correlation assessment. A Pearson Correlation matrix was developed to examine the strength of these bivariate associations between Ta, and UPs at different spatial scales represented by varying buffer sizes. Furthermore, a stepwise backward MLR was employed to examine the relationships between LST, Ta, and UPs to understand how well intra-urban variations of UHI can be explained by the UPs at effective scales.

3.1. SUHI-UHI Relation

It is well documented and recognized that nighttime Ta is the most convenient indicator of the UHI effect. Therefore, in the absence of Ta nighttime, any substitute is required to be highly consistent. In search of this consistency, we have evaluated the correlation of Ta nighttime with LST datasets. Contrary to what several studies have reported [54,55], the relationship between daytime LST and daytime Ta is stronger and more significant compared to that of the nighttime LST and nighttime Ta for the case study (Table 2). However, similar to the study by Zhang et al. [56], the model using LST nighttime performed better than the LST daytime in describing UHI. Ta nighttime was totally inconsistent with LST daytime (Table 2 (a)), which means a daytime LST may not be an excellent option to substitute for or relate to UHI (nocturnal) in the absence of a nighttime LST. Nighttime LST can be an option to infer an understanding of the UHI pattern. However, the correlation

was low to moderate and insignificant for our case (Table 2 (b)). Even if Ta daytime and LST daytime had a strong correlation in our case, Ta daytime is not a reliable indicator of UHI and, hence, is considered irrelevant. Nevertheless, the complex relationship between the Ta nighttime and LST, which manifests itself in a weak correlation, casts doubt on the use of LST to represent UHI.

Table 2. Pearson Correlation between LST daytime/nighttime and (a) Ta daytime, (b) Ta nighttime.

Ta Daytime	LST Daytime	LST Nighttime
	(a)	
Buff_25	0.430 *	0.189
Buff_50	0.453 **	0.197
Buff_75	0.484 **	0.192
Buff_100	0.518 **	0.198
Buff_125	0.521 **	0.188
Buff_150	0.541 **	0.147
Buff_175	0.559 **	0.094
Buff_200	0.566 **	0.048
Ta nighttime	LST daytime	LST nighttime
	(b)	
Buff_25	−0.036	0.103
Buff_50	−0.004	0.105
Buff_75	−0.018	0.122
Buff_100	−0.026	0.158
Buff_125	−0.012	0.199
Buff_150	−0.032	0.249
Buff_175	−0.058	0.300
Buff_200	−0.082	0.335

Pearson's $r > 0.5$ (bold), (*) Correlation is significant at 0.05 level, (**) Correlation is significant at 0.01 level.

The Ta and LST relation is observed to vary with scale. The strength of the relationship increases with the buffer size and levels out, reaching 200 m. Therefore, small buffer sizes may not be adequate to relate LST with Ta measurements.

3.2. SUHI Relation with Urban Parameters

To explore whether the SUHI effect varied together with the driving factors of SUHI, the relationship of LST was analyzed for its relationship between UPs using Pearson Correlation. According to the empirical results, daytime LST has a strong negative correlation with NDVI, as reported by most studies [63,96,111], and a strong positive correlation with Normalized Difference Built-up Index (NDBI) [96], and population density (PD). For the UPs, correlation with daytime LST grows from weak to stronger with a buffer size of up to 150–175 m (Table 3 (a)).

Nighttime LST has a strong negative correlation with NDVI and a strong positive correlation with RND and MBH. Nocturnal SUHI correlation grows from weak to stronger with a buffer size up to 150–175 m for NDBI, BVD, BFD (positively), and SVF (negatively) (Table 3 (b)).

Table 3. LST and UPs Pearson Correlations (a) for daytime LST, (b) for nighttime LST.

LST Daytime	NDVI	NDBI	Albedo	SR	MBH	BFD	BVD	SVF	PD	RND
Buff_25	−0.468 **	0.587 **	−0.032	0.114	0.140	0.077	0.037	−0.087	0.254	−0.200
Buff_50	−0.490 **	0.660 **	0.174	0.138	0.123	0.366 *	0.181	−0.199	0.527 **	−0.176
Buff_75	−0.492 **	0.647 **	0.269	0.248	−0.219	0.326	0.063	−0.214	0.493 **	−0.181
Buff_100	−0.452 **	0.628 **	0.305	0.297	−0.140	0.250	0.013	−0.208	0.493 **	−0.180
Buff_125	−0.408 *	0.592 **	0.342	0.343	−0.152	0.232	0.039	−0.220	0.515 **	−0.162
Buff_150	−0.361 *	0.542 **	0.364 *	0.347	−0.173	0.363 *	0.050	−0.188	0.503 **	−0.130
Buff_175	−0.334	0.484 **	0.371 *	0.308	−0.160	0.389 *	0.057	−0.196	0.494 **	−0.082
Buff_200	−0.300	0.430*	0.387 *	0.266	−0.163	0.374 *	0.035	−0.210	0.484 **	−0.048
(a)										
LST nighttime	NDVI	NDBI	Albedo	SR	MBH	BFD	BVD	SVF	PD	RND
Buff_25	−0.413 *	0.101	0.198	−0.184	−0.056	−0.031	−0.013	−0.074	−0.013	0.533 **
Buff_50	−0.476 **	0.067	0.089	−0.198	0.281	0.030	0.043	−0.047	0.043	0.531 **
Buff_75	−0.454 **	0.081	0.039	−0.198	0.299	0.100	0.131	−0.071	0.131	0.545 **
Buff_100	−0.459 **	0.139	0.084	−0.156	0.283	0.109	0.144	−0.118	0.144	0.552 **
Buff_125	−0.488 **	0.202	0.124	−0.130	0.422 *	0.226	0.207	−0.175	0.207	0.579 **
Buff_150	− 0.530 **	0.246	0.128	−0.121	0.500 **	0.258	0.244	−0.235	0.244	0.621 **
Buff_175	− 0.567 **	0.257	0.085	−0.138	0.530 **	0.321	0.300	−0.231	0.300	0.669 **
Buff_200	− 0.604 **	0.261	0.002	−0.165	0.594 **	0.293	0.325	−0.199	0.325	0.703 **
(b)										

Pearson's $r > 0.5$ (bold). (*) Correlation is significant at 0.05 level, (**) Correlation is significant at 0.01 level.

3.3. UHI Relation with Urban Parameters

According to the empirical results for UHI and UPs relationship, T_a daytime has a strong positive correlation with albedo. UHI daytime is correlated with SR and PD positively but not significantly. UHI diurnal, being negatively correlated with MBH, BVD, and RND, is questionable. It is considered that shading is effective where open impermeable spaces are more prone to diurnal UHI effects. This contradiction also manifests in a positive, strong correlation with albedo contrary to the reported negative correlation [112,113]. Higher albedo surfaces typically reduce absorbed radiation; hence, they are usually cooler (Table 4 (a)).

T_a nighttime is a reliable indicator of UHI; therefore, it is of critical importance to assess nighttime T_a and its driving factors. T_a nighttime has a strong negative correlation with NDVI and the SVF. It has a strong positive correlation with NDBI, BVD, RND, MBH, and BFD (Table 4 (b)). The NDVI relationship with UHI is well documented in the literature. SVF is also documented to be closely associated with nocturnal UHI. The SVF varies from 1 for completely unobstructed land surface to 0 for completely obstructed land surface by the buildings. As the sky view reduces, the heat gets trapped, and cooling is prevented. Buildings absorb thermal energy from the sun and continue to release it during the night. BFD, MBH, and BVD are indicators of how dense the buildings are horizontally, vertically, and volumetrically, respectively. The energy emitted as heat grows with the building materials that store energy are greater in surface and volume. Moreover, traffic activities represented with proxy variable RND are very influential on UHI. Emissions and heat released from the vehicles are considered responsible for the additional heat introduced to the ambient temperature.

Correlation analysis shows clearly that the spatial scale described with buffer size is effective on the relationship between the SUHI, UHI, and the UPs. As quantified by the correlation coefficients of these relationships, the magnitude of UPs increased with the increasing buffer size, e.g., the buffer size as small as 25 m, including a few pixels of 30 m resolution UPs, is not capturing the spatial scale. However, the increase in correlation with

buffer size is not steady, and there is an extent to which the correlation levels out. The size of the buffer where correlation levels out, that is, it starts to drop or increase very slowly, is considered a critical buffer width for the case study. Accordingly, around 150–175 m represents a critical buffer size for SUHI, and 125 m represents a critical buffer size for UHI in relation to UPs. Studies also indicate that UHI is better correlated in at least 100 m proximity, e.g., SVF around 100 m buffer [114].

Table 4. Ta and UPs Pearson Correlations (a) for daytime Ta, (b) for nighttime Ta.

Ta Daytime	NDVI	NDBI	Albedo	SR	MBH	BFD	BVD	SVF	PD	RND
Buff_25	−0.201	0.129	0.188	0.392 *	−0.242	−0.185	−0.289	0.085	0.195	−0.340
Buff_50	−0.112	0.194	0.264	0.329	−0.097	−0.001	−0.199	0.130	0.306	−0.332
Buff_75	−0.096	0.176	0.346	0.310	−0.274	−0.041	−0.268	0.094	0.234	−0.326
Buff_100	−0.085	0.167	0.393 *	0.291	−0.197	−0.146	−0.315	0.155	0.188	−0.322
Buff_125	−0.107	0.158	0.461 **	0.282	−0.212	−0.255	−0.369 *	0.160	0.141	−0.312
Buff_150	−0.108	0.143	0.456 **	0.272	−0.221	−0.142	−0.278	0.163	0.175	−0.302
Buff_175	−0.116	0.145	0.485 **	0.288	−0.227	−0.085	−0.257	0.138	0.197	−0.288
Buff_200	−0.102	0.139	0.526 **	0.300	−0.231	−0.081	−0.273	0.120	0.215	−0.276
(a)										
Ta nighttime	NDVI	NDBI	Albedo	SR	MBH	BFD	BVD	SVF	PD	RND
Buff_25	−0.237	0.460 **	−0.159	0.031	0.654 **	0.699 **	0.684 **	−0.704 **	0.308	0.582 **
Buff_50	−0.383 *	0.406 *	−0.196	0.061	0.668 **	0.687 **	0.779 **	−0.782 **	0.318	0.576 **
Buff_75	−0.416 *	0.482 **	−0.277	0.082	0.645 **	0.683 **	0.826 **	−0.756 **	0.379 *	0.573 **
Buff_100	−0.442 *	0.493 **	−0.270	0.128	0.419 *	0.731 **	0.839 **	−0.771 **	0.400 *	0.573 **
Buff_125	−0.471 **	0.498 **	−0.224	0.142	0.447 *	0.729 **	0.841 **	−0.762 **	0.422 *	0.573 **
Buff_150	−0.480 **	0.503 **	−0.156	0.168	0.439 *	0.634 **	0.816 **	−0.711 **	0.366 *	0.572 **
Buff_175	−0.467 **	0.488 **	−0.091	0.170	0.387 *	0.615 **	0.793 **	−0.625 **	0.303	0.566 **
Buff_200	−0.440 *	0.452 **	−0.096	0.171	0.321	0.602 **	0.764 **	−0.518 **	0.241	0.557 **
(b)										

Pearson's $r > 0.5$ (bold). (*) Correlation is significant at 0.05 level, (**) Correlation is significant at 0.01 level.

For a better understanding of the relationship between UHI and UPs and to explore how UPs are effective in estimating UHI, a LUR extension of MLR was implemented. As nighttime UHI describes the UHI effect and UHI is observed stronger at night than during the day, LUR was implemented to estimate nighttime Ta based on UPs. Many studies utilize LST for UHI estimation. However, as the correlation between the nighttime Ta and LST was not strong for the case study, the LST was not employed as a predictor. Ta nighttime (32 measurements) as a dependent variable and UPs mean statistics for 125 m buffer (critical buffer size) were employed as independent explanatory variables. In prior checks for correlation and multicollinearity, albedo and SR were removed owing to their weak correlation with nighttime UHI. Among NDVI and NDBI, the latter was removed for collinearity $VIF > 10$ and $p > 0.1$. The lack of NDBI can be compensated with other parameters, e.g., BFD and SVF, that may well describe the built-up environment. A stepwise backward MLR adopting LUR was conducted on eight variables, namely, NDVI, NDBI, MBH, BFD, BVD, SVF, PD, and RND. The backward model eliminates BFD, PD, NDVI, and MBH, respectively, leaving SVF, BVD, and RND as predictor variables with an adjusted coefficient of determination, R^2 of 0.688. Regression statistics reveal that SVF is the most influential factor that drives UHI, the BVD follows, finally comes RND with standardized Beta Coefficients of -0.411 , 0.333 , and 0.212 , respectively. SVF has a strong negative relationship with UHI, where the decreasing SVF values cause heat to be trapped and lead to an increased Ta. An increase in BVD per unit contributes to UHI formation. Similarly,

with the rise in RND per unit that is a proxy to traffic density, Ta tends to increase. Other UPs, although, may contribute to UHI, their influence is slight compared to the three parameters captured by the model.

The linear equation of MLR using spatial LUR modeling is as follows:

$$Ta_i = \beta_0 + \beta_1 Var_{i1} + \dots + \beta_n var_{in} + \varepsilon \quad (3)$$

where Ta_i is the observed Ta nighttime at location i , β_0 is the constant (intercept), β_n are coefficients of UPs, $n = 3$, and ε is the model's error term (the residual). R^2 of approximately 0.65–0.75 is considered a good model performance in UHI estimation studies [38]. In the present study, the variability of Ta explained by SVF , BVD , and RND , with R^2 of 0.69 is a good model performance. Ta for the case study can be estimated using the following linear equation with a Standard Error of Estimate (SEE) of 0.57:

$$Ta_i = 23.531 - 1.986 \times SVF_i + 5.283E - 6 \times BVD_i + 0.029 \times RND_i \quad (4)$$

3.4. SUHI, UHI Diurnal Changes

Most studies use daytime or nighttime Ta measurements or LST interchangeably to describe the UHI phenomenon in urban environments. However, both Ta and LST for day and night may show considerable changes. This part of the study is devoted to understanding the relationship between LST daytime vs. nighttime and UHI daytime vs. nighttime based on their correlation statistics.

The Pearson Correlation between LST daytime, calculated from Landsat 8, and LST nighttime from ASTER thermal product is 0.251, $p = 0.167$ for buffer size 150. Although there is a positive correlation, it is weak and statistically not significant.

For UHI diurnal comparisons, 26 Ta nighttime and daytime coherent measurements from the same locations were found to have a weak positive correlation of 0.248 (not significant, $p = 0.223$). To further examine this questionably low correlation, the dot plot of Ta daytime and Ta nighttime was evaluated. Accordingly, the daytime and nighttime Ta show low–low, high–high, and low–high clusters of Ta day and night. The weak correlation between Ta daytime and Ta nighttime is mainly attributed to the low–high cluster that spoils the linear coherence between the measurements and, hence, worth further inspection. The low–low, high–high, and low–high clusters' member points were colored in blue, yellow, and red, respectively, in both the dot plot and the map (Figure 6). The mean statistics of the points that represent each region for the UPs are given in Table 5.

- (i) In the blue region, the temperatures are relatively low for both day and night. Corresponding measurement locations refer to a region characterized by vegetation and tree abundance (high NDVI) with relatively low building footprint and volume density (BFD, BVD), low-rise buildings (low MBH), and an increased SVF. This low-density fabric of residential use at the urban fringes does not get as warm as the other two regions.
- (ii) In the yellow region, the temperatures are relatively high for both day and night. Corresponding measurement locations refer to a region that is a concentrated built-up land mainly composed of residential use and was subject to haphazard development. A moderate score of MBH, BFD, BVD, SVF, and RND, accompanied with scarce green areas and trees (low NDVI), and high NDBI results in relatively high temperatures for both day and night.
- (iii) The red region is not very warm during the day, but the warmest at night. This is the urban core with the commercial, financial, educational functions, and health facilities. The built environment is characterized by a high building footprint, volume density, and high-rise buildings (BFD, BVD, MBH) where SVF is small. However, there is an ample number of big trees, especially along the walking lanes, that is represented with a moderate NDVI. The relatively low daytime temperatures are mainly attributed to the shadow effect due to high-rise buildings and large trees that may prevent an increase in temperatures during the daytime. However, at nighttime, due to the

high building density and volume, the heat is stored and re-emitted; and due to the low SVF, heat is trapped and, hence, cooling at night is prevented. Traffic that is represented with high RND is considered another factor that introduces additional heat to the ambient temperatures at night as this part of the city core is active at night (Table 5).

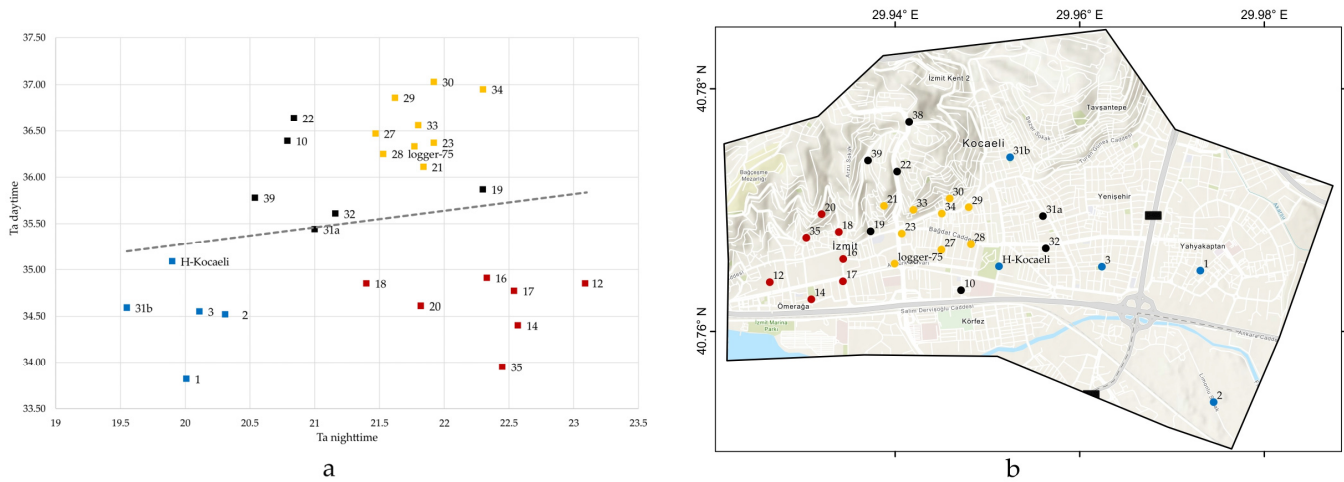


Figure 6. Daytime and nighttime air temperature comparisons: (a) Ta daytime–Ta nighttime dot plot; (b) Ta measurement locations. Colors show clusters of the Ta daytime and Ta nighttime.

Table 5. UPs mean values for city regions (blue, yellow, red) and UPs minimum and maximum values. Highest scores per urban parameter were shown bold.

	Ta Point Id	NDVI	NDBI	MBH	BFD	BVD	SVF	PD	RND
Blue	1,2,3, 31b, H-Kocaeli	0.326	−0.0703	7.770	0.220	2225.66	0.871	83.16	9.921
Yellow	21, 23, 27, 28, 29, 30, 33, 34, log-75	0.214	0.044	10.535	0.397	4744.6	0.697	251.94	12.09
Red	12, 14, 16, 17, 18, 20, 35	0.277	0.032	12.212	0.462	5408.74	0.621	221.91	16.173
Min.	-	0.134	−0.183	0	0.028	900	0.588	0	2.111
Max.	-	0.454	0.091	16.75	0.559	8180.36	0.999	383.19	21.492

4. Conclusions

The present study aims to provide a basic dataset that can be simply acquired or calculated and proposes straightforward methods and basic statistical tools to explore the relationships between data and the parameters very commonly employed in urban climate studies. In urban climate research, most studies employ LST as a substitute for UHI without much questioning. However, results from the present study reveal that LST is not a very good indicator of UHI. Therefore, more care should be taken when substituting UHI with LST. Daytime LST, in particular, should be cautiously used in climate studies as UHI is characterized by nighttime Ta and commonly used daytime LST can mislead the strategies and critical measures to be taken. In the absence of any Ta nighttime measurements of fine spatial distribution, the use of nighttime LST might be a better option, albeit with a possible low to moderate correlation with Ta nighttime. Empirical results show that UPs better explain UHI variation and are considered a better option to estimate UHI in the absence of densely distributed Ta.

The increase in artificial surfaces and building structures due to urbanization has a significant impact on the increase in the UHI effect. The SVF, BVD, and RND, respectively, were the most related parameters with nighttime Ta, which is the determinant of the UHI phenomenon. Volumetric buildings and reduced sky view within a pattern of narrow streets, coupled with traffic intensity, establishes the most favorable conditions for the

increased UHI effect. The LUR model can estimate the intra-urban UHI effect given relevant UPs at an effective scale represented with a critical buffer size. With the increased availability of city models and building data, many of the UP data can be easily retrieved and used for UHI modeling.

Similar to the discrepancy between daytime and nighttime LST, T_a measurements do not correspond very well for day and night and have a low correlation. This inconsistency can be attributed to the relatively higher T_a nighttime observations specific to a particular region in the city. In these typical regions, the cooling is considered to be prevented, and traffic contributes to the heating. These localities should be of prior interest in developing urban cooling strategies at the urban design scale.

Contrary to a growing number of studies that employ remotely sensed LST, owing to the lack of spatially detailed T_a data in cities, our findings highlight that T_a is indispensable for precise mapping and accurate description of the UHI effect. LST that characterizes SUHI, on the other hand, can be a proxy for studies that aim to map LST that is intricately related to UHI. A microscale analysis of UHI for a comprehensive understanding of how various UPs are related to urban air temperature variations is of crucial importance for urban planning and design with a focus on UHI mitigation. UHI modeling based on T_a measurements that are densely distributed is the primary reference metric for UHI. However, the most influential UPs can also represent the UHI effect in this aim. Decision makers should consider the localities of the highest intensity of UHI described by T_a or estimated by UPS for taking specific measures to reduce exposure, especially during heat waves. Urban planners and designers with the knowledge of the degree of influence of UPs for UHI in their case study can establish decent strategies for reducing the UPs' particular contribution to UHI.

Author Contributions: Conceptualization, D.G.; methodology, D.G. and İ.T.G.; software, D.G. and İ.T.G.; validation, İ.T.G.; formal analysis, D.G.; investigation, D.G.; resources, D.G.; data curation, İ.T.G.; writing—original draft preparation, D.G.; writing—review and editing, D.G.; visualization, İ.T.G.; supervision, D.G.; project administration, D.G.; funding acquisition, D.G. and İ.T.G. All authors have read and agreed to the published version of the manuscript.

Funding: This study was funded by Kocaeli Metropolitan Municipality and Kocaeli University Technology Transfer Office under the project “Urban Quality of Life Assessment in Kocaeli Province Izmit District” (project id: 2018-01.08.201).

Informed Consent Statement: Informed consent was obtained from all subjects involved in the study.

Data Availability Statement: The data of the study are available upon request. Some data are not publicly available due to the funding institution's legislation on data protection.

Conflicts of Interest: The authors declare no conflict of interest.

References

1. The United Nations. *World Urbanization Prospects: The 2018 Revision*; United Nations Department of Economic and Social Affairs, Population Division: New York, NY, USA, 2019.
2. Kalnay, E.; Cai, M. Impact of urbanization and land-use change on climate. *Nature* **2003**, *423*, 528–531. [[CrossRef](#)]
3. Stewart, I.D. A systematic review and scientific critique of methodology in modern urban heat island literature. *Int. J. Climatol.* **2011**, *31*, 200–217. [[CrossRef](#)]
4. DeFries, R. Terrestrial vegetation in the coupled human-earth system: Contributions of remote sensing. *Annu. Rev. Environ. Resour.* **2008**, *33*, 369–390. [[CrossRef](#)]
5. Zhou, B.; Kaplan, S.; Peeters, A.; Kloog, I.; Erell, E. “Surface”, “satellite” or “simulation”: Mapping intra-urban microclimate variability in a desert city. *Int. J. Climatol.* **2020**, *40*, 3099–3117. [[CrossRef](#)]
6. Yan, Y.Y. The influence of weather on human mortality in Hong Kong. *Soc. Sci. Med.* **2000**, *50*, 419–427. [[CrossRef](#)] [[PubMed](#)]
7. Anderson, B.G.; Bell, M.L. Weather-related mortality: How heat, cold, and heat waves affect mortality in the United States. *Epidemiology* **2009**, *20*, 205. [[CrossRef](#)]
8. Song, J.; Yu, H.; Lu, Y. Spatial-scale dependent risk factors of heat-related mortality: A multiscale geographically weighted regression analysis. *Sustain. Cities Soc.* **2021**, *74*, 103159. [[CrossRef](#)]
9. Čeplová, N.; Kalusová, V.; Lososová, Z. Effects of settlement size, urban heat island and habitat type on urban plant biodiversity. *Landsc. Urban Plan.* **2017**, *159*, 15–22. [[CrossRef](#)]

10. Sarrat, C.; Lemonsu, A.; Masson, V.; Guédalia, D. Impact of urban heat island on regional atmospheric pollution. *Atmos. Environ.* **2006**, *40*, 1743–1758. [CrossRef]
11. Briciu, A.-E.; Mihăilă, D.; Graur, A.; Oprea, D.I.; Prisăcariu, A.; Bistricean, P.I. Changes in the water temperature of rivers impacted by the urban heat island: Case study of Suceava city. *Water* **2020**, *12*, 1343. [CrossRef]
12. Santamouris, M.; Papanikolaou, N.; Livada, I.; Koronakis, I.; Georgakis, C.; Argiriou, A.; Assimakopoulos, D. On the impact of urban climate on the energy consumption of buildings. *Sol. Energy* **2001**, *70*, 201–216. [CrossRef]
13. Salamanca, F.; Georgescu, M.; Mahalov, A.; Moustou, M.; Wang, M.; Svoma, B. Assessing summertime urban air conditioning consumption in a semiarid environment. *Environ. Res. Lett.* **2013**, *8*, 034022. [CrossRef]
14. Litardo, J.; Palme, M.; Borbor-Córdova, M.; Caiza, R.; Macías, J.; Hidalgo-León, R.; Soriano, G. Urban Heat Island intensity and buildings' energy needs in Duran, Ecuador: Simulation studies and proposal of mitigation strategies. *Sustain. Cities Soc.* **2020**, *62*, 102387. [CrossRef]
15. Bloomberg, M. Cities Have Played a More Important Role in Shaping the World than Empires. Available online: <https://espas.secure.europarl.europa.eu/orbis/document/global-trends-2030-future-urbanization-and-megacities-0> (accessed on 30 October 2023).
16. Meehl, G.A.; Tebaldi, C. More intense, more frequent, and longer lasting heat waves in the 21st century. *Science* **2004**, *305*, 994–997. [CrossRef] [PubMed]
17. Li, D.; Bou-Zeid, E. Synergistic interactions between urban heat islands and heat waves: The impact in cities is larger than the sum of its parts. *J. Appl. Meteorol. Climatol.* **2013**, *52*, 2051–2064. [CrossRef]
18. Oke, T.R. The energetic basis of the urban heat island. *Q. J. R. Meteorol. Soc.* **1982**, *108*, 1–24. [CrossRef]
19. Aletba, S.R.O.; Hassan, N.A.; Jaya, R.P.; Aminudin, E.; Mahmud, M.Z.H.; Mohamed, A.; Hussein, A.A. Thermal performance of cooling strategies for asphalt pavement: A state-of-the-art review. *J. Traffic Transp. Eng. (Engl. Ed.)* **2021**, *8*, 356–373. [CrossRef]
20. Oke, T.R. Canyon geometry and the nocturnal urban heat island: Comparison of scale model and field observations. *J. Climatol.* **1981**, *1*, 237–254. [CrossRef]
21. Taha, H. Urban climates and heat islands: Albedo, evapotranspiration, and anthropogenic heat. *Energy Build.* **1997**, *25*, 99–103. [CrossRef]
22. Klysik, K.; Fortuniak, K. Temporal and spatial characteristics of the urban heat island of Łódź, Poland. *Atmos. Environ.* **1999**, *33*, 3885–3895. [CrossRef]
23. Yan, H.; Fan, S.; Guo, C.; Hu, J.; Dong, L. Quantifying the impact of land cover composition on intra-urban air temperature variations at a mid-latitude city. *PLoS ONE* **2014**, *9*, e102124. [CrossRef]
24. Zhou, B.; Rybski, D.; Kropp, J.P. On the statistics of urban heat island intensity. *Geophys. Res. Lett.* **2013**, *40*, 5486–5491. [CrossRef]
25. Oke, R. Urban climate and global environmental change. In *Applied Climatology*; Routledge: Abingdon, UK, 1997; pp. 273–287.
26. Oke, T.R.; Mills, G.; Christen, A.; Voogt, J.A. *Urban Climates*; Cambridge University Press: Cambridge, UK, 2017.
27. Buyantuyev, A.; Wu, J. Urban heat islands and landscape heterogeneity: Linking spatiotemporal variations in surface temperatures to land-cover and socioeconomic patterns. *Landsc. Ecol.* **2010**, *25*, 17–33. [CrossRef]
28. Oke, T.R. The distinction between canopy and boundary-layer urban heat islands. *Atmosphere* **1976**, *14*, 268–277. [CrossRef]
29. Williams, T.B. Microclimatic temperature relationships over different surfaces. *J. Geogr.* **1991**, *90*, 285–291. [CrossRef]
30. Yang, S.; Wang, L.L.; Stathopoulos, T.; Marey, A.M. Urban microclimate and its impact on built environment—A review. *Build. Environ.* **2023**, *238*, 110334. [CrossRef]
31. Parsaee, M.; Joybari, M.M.; Mirzaei, P.A.; Haghighat, F. Urban heat island, urban climate maps and urban development policies and action plans. *Environ. Technol. Innov.* **2019**, *14*, 100341. [CrossRef]
32. Unger, J.; Savić, S.; Gál, T. Modelling of the annual mean urban heat island pattern for planning of representative urban climate station network. *Adv. Meteorol.* **2011**, *2011*, 398613. [CrossRef]
33. Peng, W.; Wang, R.; Duan, J.; Gao, W.; Fan, Z. Surface and canopy urban heat islands: Does urban morphology result in the spatiotemporal differences? *Urban Clim.* **2022**, *42*, 101136. [CrossRef]
34. Arnfield, A.J. Two decades of urban climate research: A review of turbulence, exchanges of energy and water, and the urban heat island. *Int. J. Climatol. A J. R. Meteorol. Soc.* **2003**, *23*, 1–26. [CrossRef]
35. Oke, T. *Boundary Layer Climates*; Routledge: London, UK, 1987; 464p.
36. Rizwan, A.M.; Dennis, L.Y.; Chunho, L. A review on the generation, determination and mitigation of Urban Heat Island. *J. Environ. Sci.* **2008**, *20*, 120–128. [CrossRef]
37. Voogt, J.A.; Oke, T.R. Thermal remote sensing of urban climates. *Remote Sens. Environ.* **2003**, *86*, 370–384. [CrossRef]
38. Shi, Y.; Katschner, L.; Ng, E. Modelling the fine-scale spatiotemporal pattern of urban heat island effect using land use regression approach in a megacity. *Sci. Total Environ.* **2018**, *618*, 891–904. [CrossRef] [PubMed]
39. Zhang, Y.; Zhang, J.; Zhang, X.; Zhou, D.; Gu, Z. Analyzing the characteristics of UHI (Urban heat island) in summer daytime based on observations on 50 sites in 11 LCZ (local climate zone) types in Xi'an, China. *Sustainability* **2021**, *13*, 83. [CrossRef]
40. Oke, T.R. *Initial Guidance to Obtain Representative Meteorological Observations at Urban Sites*; World Meteorological Organization: Geneva, Switzerland, 2004; Volume 81.
41. Schlünzen, K.H.; Grimmond, S.; Baklanov, A. *Guidance to Measuring, Modelling and Monitoring the Canopy Layer Urban Heat Island (CL-UHI)*; World Meteorological Organization: Geneva, Switzerland, 2023.
42. Gubler, M.; Christen, A.; Remund, J.; Brönnimann, S. Evaluation and application of a low-cost measurement network to study intra-urban temperature differences during summer 2018 in Bern, Switzerland. *Urban Clim.* **2021**, *37*, 100817. [CrossRef]

43. Alvi, U.; Suomi, J.; Käyhkö, J. A cost-effective method for producing spatially continuous high-resolution air temperature information in urban environments. *Urban Clim.* **2022**, *42*, 101123. [[CrossRef](#)]
44. Yuan, F.; Bauer, M.E. Comparison of impervious surface area and normalized difference vegetation index as indicators of surface urban heat island effects in Landsat imagery. *Remote Sens. Environ.* **2007**, *106*, 375–386. [[CrossRef](#)]
45. Yang, Y.; Endreny, T.A.; Nowak, D.J. A physically based analytical spatial air temperature and humidity model. *J. Geophys. Res. Atmos.* **2013**, *118*, 10449–10463. [[CrossRef](#)]
46. Acosta, M.P.; Vahdatikhaki, F.; Santos, J.; Hammad, A.; Dorée, A.G. How to bring UHI to the urban planning table? A data-driven modeling approach. *Sustain. Cities Soc.* **2021**, *71*, 102948. [[CrossRef](#)]
47. Roth, M.; Oke, T.R.; Emery, W.J. Satellite-derived urban heat islands from three coastal cities and the utilization of such data in urban climatology. *Int. J. Remote Sens.* **1989**, *10*, 1699–1720. [[CrossRef](#)]
48. Schwarz, N.; Schlink, U.; Franck, U.; Großmann, K. Relationship of land surface and air temperatures and its implications for quantifying urban heat island indicators—An application for the city of Leipzig (Germany). *Ecol. Indic.* **2012**, *18*, 693–704. [[CrossRef](#)]
49. Mostovoy, G.V.; King, R.L.; Reddy, K.R.; Kakani, V.G.; Filippova, M.G. Statistical estimation of daily maximum and minimum air temperatures from MODIS LST data over the state of Mississippi. *GIScience Remote Sens.* **2006**, *43*, 78–110. [[CrossRef](#)]
50. Kloog, I.; Chudnovsky, A.; Koutrakis, P.; Schwartz, J. Temporal and spatial assessments of minimum air temperature using satellite surface temperature measurements in Massachusetts, USA. *Sci. Total Environ.* **2012**, *432*, 85–92. [[CrossRef](#)]
51. Pelta, R.; Chudnovsky, A.A.; Schwartz, J. Spatio-temporal behavior of brightness temperature in Tel-Aviv and its application to air temperature monitoring. *Environ. Pollut.* **2016**, *208*, 153–160. [[CrossRef](#)]
52. Xiong, Y.; Chen, F. Correlation analysis between temperatures from Landsat thermal infrared retrievals and synchronous weather observations in Shenzhen, China. *Remote Sens. Appl. Soc. Environ.* **2017**, *7*, 40–48. [[CrossRef](#)]
53. Azevedo, J.A.; Chapman, L.; Muller, C.L. Quantifying the daytime and night-time urban heat island in Birmingham, UK: A comparison of satellite derived land surface temperature and high resolution air temperature observations. *Remote Sens.* **2016**, *8*, 153. [[CrossRef](#)]
54. Hartz, D.; Prashad, L.; Hedquist, B.; Golden, J.; Brazel, A. Linking satellite images and hand-held infrared thermography to observed neighborhood climate conditions. *Remote Sens. Environ.* **2006**, *104*, 190–200. [[CrossRef](#)]
55. Del Pozo, S.; Landes, T.; Nerry, F.; Kastendeuch, P.; Najjar, G.; Philipps, N.; Lagüela, S. UHI estimation based on ASTER and MODIS satellite imagery: First results on Strasbourg city, France. *Int. Arch. Photogramm. Remote Sens. Spat. Inf. Sci.* **2020**, *43*, 799–805. [[CrossRef](#)]
56. Zhang, W.; Huang, Y.; Yu, Y.; Sun, W. Empirical models for estimating daily maximum, minimum and mean air temperatures with MODIS land surface temperatures. *Int. J. Remote Sens.* **2011**, *32*, 9415–9440. [[CrossRef](#)]
57. Stewart, I.D. Landscape representation and the urban-rural dichotomy in empirical urban heat island literature, 1950–2006. *Acta Climatol. Chorol.* **2007**, *40*, 111–121.
58. Sharpe, D.M. Microclimatology. In *Climatology*; Springer: Boston, MA, USA, 1987; pp. 572–581. [[CrossRef](#)]
59. Anderson, S. *An Evaluation of Spatial Interpolation Methods on Air Temperature in Phoenix, AZ*; Department of Geography, Arizona State University: Tempe, AZ, USA, 2002; Volume 104.
60. Li, D.; Bou-Zeid, E.; Oppenheimer, M. The effectiveness of cool and green roofs as urban heat island mitigation strategies. *Environ. Res. Lett.* **2014**, *9*, 055002. [[CrossRef](#)]
61. Garuma, G.F. Review of urban surface parameterizations for numerical climate models. *Urban Clim.* **2018**, *24*, 830–851. [[CrossRef](#)]
62. Aslan, N.; Koc-San, D. The use of land cover indices for rapid surface urban heat island detection from multi-temporal Landsat imageries. *ISPRS Int. J. Geo-Inf.* **2021**, *10*, 416. [[CrossRef](#)]
63. Okumus, D.E.; Terzi, F. Evaluating the role of urban fabric on surface urban heat island: The case of Istanbul. *Sustain. Cities Soc.* **2021**, *73*, 103128. [[CrossRef](#)]
64. Yang, L.; Yu, K.; Ai, J.; Liu, Y.; Yang, W.; Liu, J. Dominant factors and spatial heterogeneity of land surface temperatures in urban areas: A case study in Fuzhou, China. *Remote Sens.* **2022**, *14*, 1266. [[CrossRef](#)]
65. Kiavarz, M.; Hosseinbeigi, S.B.; Mijani, N.; Shahsavary, M.S.; Firozjaei, M.K. Predicting spatial and temporal changes in surface urban heat islands using multi-temporal satellite imagery: A case study of Tehran metropolis. *Urban Clim.* **2022**, *45*, 101258. [[CrossRef](#)]
66. Wang, X.; Zhang, Y.; Yu, D. Exploring the Relationships between Land Surface Temperature and Its Influencing Factors Using Multisource Spatial Big Data: A Case Study in Beijing, China. *Remote Sens.* **2023**, *15*, 1783. [[CrossRef](#)]
67. Gerçek, D.; Güven, İ.; Oktay, İ. Analysis of the intra-city variation of urban heat island and its relation to land surface/cover parameters. *ISPRS Ann. Photogramm. Remote Sens. Spat. Inf. Sci.* **2016**, *3*, 123–129. [[CrossRef](#)]
68. Ramírez-Aguilar, E.A.; Souza, L.C.L. Urban form and population density: Influences on Urban Heat Island intensities in Bogotá, Colombia. *Urban Clim.* **2019**, *29*, 100497. [[CrossRef](#)]
69. Foissard, X.; Dubreuil, V.; Quénot, H. Defining scales of the land use effect to map the urban heat island in a mid-size European city: Rennes (France). *Urban Clim.* **2019**, *29*, 100490. [[CrossRef](#)]
70. Puche, M.; Vavassori, A.; Brovelli, M.A. Insights into the Effect of Urban Morphology and Land Cover on Land Surface and Air Temperatures in the Metropolitan City of Milan (Italy) Using Satellite Imagery and In Situ Measurements. *Remote Sens.* **2023**, *15*, 733. [[CrossRef](#)]

71. Liu, Y.; Xu, Y.; Zhang, Y.; Han, X.; Weng, F.; Xuan, C.; Shu, W. Impacts of the Urban Spatial Landscape in Beijing on Surface and Canopy Urban Heat Islands. *J. Meteorol. Res.* **2022**, *36*, 882–899. [[CrossRef](#)]
72. Swaid, H. Urban climate effects of artificial heat sources and ground shadowing by buildings. *Int. J. Climatol.* **1993**, *13*, 797–812. [[CrossRef](#)]
73. Stewart, I.D.; Oke, T.R. Local climate zones for urban temperature studies. *Bull. Am. Meteorol. Soc.* **2012**, *93*, 1879–1900. [[CrossRef](#)]
74. Georgescu, M.; Chow, W.T.; Wang, Z.; Brazel, A.; Trapido-Lurie, B.; Roth, M.; Benson-Lira, V. Prioritizing urban sustainability solutions: Coordinated approaches must incorporate scale-dependent built environment induced effects. *Environ. Res. Lett.* **2015**, *10*, 061001. [[CrossRef](#)]
75. Xu, D.; Zhou, D.; Wang, Y.; Meng, X.; Chen, W.; Yang, Y. Temporal and spatial variations of urban climate and derivation of an urban climate map for Xi'an, China. *Sustain. Cities Soc.* **2020**, *52*, 101850. [[CrossRef](#)]
76. Van Hove, L.; Jacobs, C.; Heusinkveld, B.; Elbers, J.; Van Driel, B.; Holtslag, A. Temporal and spatial variability of urban heat island and thermal comfort within the Rotterdam agglomeration. *Build. Environ.* **2015**, *83*, 91–103. [[CrossRef](#)]
77. Öztürk, M.Z.; Çetinkaya, G.; Aydın, S. Köppen-Geiger iklim sınıflandırmasına göre Türkiye'nin iklim tipleri. *Coğrafya Derg.* **2017**, *35*, 17–27. [[CrossRef](#)]
78. Gillespie, A.R.; Rokugawa, S.; Hook, S.J.; Matsunaga, T.; Kahle, A.B. *Temperature/Emissivity Separation Algorithm Theoretical Basis Document*; Version 2.4; ATBD Contract NAS5-31372; NASA: Washington, DC, USA, 1999.
79. Amorim, M.C.d.C.T.; Dubreuil, V.; Amorim, A.T. Day and night surface and atmospheric heat islands in a continental and temperate tropical environment. *Urban Clim.* **2021**, *38*, 100918. [[CrossRef](#)]
80. Beck, C.; Straub, A.; Breitner, S.; Cyrus, J.; Philipp, A.; Rathmann, J.; Schneider, A.; Wolf, K.; Jacobeit, J. Air temperature characteristics of local climate zones in the Augsburg urban area (Bavaria, Southern Germany) under varying synoptic conditions. *Urban Clim.* **2018**, *25*, 152–166. [[CrossRef](#)]
81. Brandsma, T.; Wolters, D. Measurement and statistical modeling of the urban heat island of the city of Utrecht (The Netherlands). *J. Appl. Meteorol. Climatol.* **2012**, *51*, 1046–1060. [[CrossRef](#)]
82. Xu, D.; Zhou, D.; Wang, Y.; Xu, W.; Yang, Y. Field measurement study on the impacts of urban spatial indicators on urban climate in a Chinese basin and static-wind city. *Build. Environ.* **2019**, *147*, 482–494. [[CrossRef](#)]
83. Kestrel Manuals. Available online: <https://www.kestrel.com.tr/uploads/dokuman/teknik-ozellikler---kestrel-1000-4500-ingilizce-95748.pdf> (accessed on 30 October 2023).
84. Kestrel Specifications. Available online: <https://www.kestrel.com.tr/uploads/dokuman/kullanma-talimatlari---kestrel-1000-3500-ingilizce-65097.pdf> (accessed on 30 October 2023).
85. Zhao, C.; Jensen, J.; Weng, Q.; Weaver, R. A geographically weighted regression analysis of the underlying factors related to the surface urban heat island phenomenon. *Remote Sens.* **2018**, *10*, 1428. [[CrossRef](#)]
86. Brunzell, N.A.; Gillies, R.R. Incorporating surface emissivity into a thermal atmospheric correction. *Photogramm. Eng. Remote Sens.* **2002**, *68*, 1263–1270.
87. Sobrino, J.A.; Jiménez-Muñoz, J.C.; Sòria, G.; Romaguera, M.; Guanter, L.; Moreno, J.; Plaza, A.; Martínez, P. Land surface emissivity retrieval from different VNIR and TIR sensors. *IEEE Trans. Geosci. Remote Sens.* **2008**, *46*, 316–327. [[CrossRef](#)]
88. Atmospheric Correction Parameter Calculator. Available online: <http://atmcorr.gsfc.nasa.gov/> (accessed on 30 October 2023).
89. Liu, L.; Lin, Y.; Liu, J.; Wang, L.; Wang, D.; Shui, T.; Chen, X.; Wu, Q. Analysis of local-scale urban heat island characteristics using an integrated method of mobile measurement and GIS-based spatial interpolation. *Build. Environ.* **2017**, *117*, 191–207. [[CrossRef](#)]
90. Leconte, F.; Bouyer, J.; Claverie, R.; Pétrissans, M. Using Local Climate Zone scheme for UHI assessment: Evaluation of the method using mobile measurements. *Build. Environ.* **2015**, *83*, 39–49. [[CrossRef](#)]
91. Ismaila, A.-R.B.; Muhammed, I.; Adamu, B. Modelling land surface temperature in urban areas using spatial regression models. *Urban Clim.* **2022**, *44*, 101213. [[CrossRef](#)]
92. Lu, L.; Weng, Q.; Xiao, D.; Guo, H.; Li, Q.; Hui, W. Spatiotemporal variation of surface urban heat islands in relation to land cover composition and configuration: A multi-scale case study of Xi'an, China. *Remote Sens.* **2020**, *12*, 2713. [[CrossRef](#)]
93. Back, Y.; Bach, P.M.; Jasper-Tönnies, A.; Rauch, W.; Kleidorfer, M. A rapid fine-scale approach to modelling urban bioclimatic conditions. *Sci. Total Environ.* **2021**, *756*, 143732. [[CrossRef](#)]
94. Ghosh, S.; Kumar, D.; Kumari, R. Assessing spatiotemporal dynamics of land surface temperature and satellite-derived indices for new town development and suburbanization planning. *Urban Gov.* **2022**, *2*, 144–156. [[CrossRef](#)]
95. Zhu, R.; Dong, X.; Wong, M.S. Estimation of the urban heat island effect in a reformed urban district: A scenario-based study in Hong Kong. *Sustainability* **2022**, *14*, 4409. [[CrossRef](#)]
96. Guha, S.; Govil, H.; Gill, N.; Dey, A. Analytical study on the relationship between land surface temperature and land use/land cover indices. *Ann. GIS* **2020**, *26*, 201–216. [[CrossRef](#)]
97. Liang, S. Narrowband to broadband conversions of land surface albedo I: Algorithms. *Remote Sens. Environ.* **2001**, *76*, 213–238. [[CrossRef](#)]
98. Kuang, W.; Liu, A.; Dou, Y.; Li, G.; Lu, D. Examining the impacts of urbanization on surface radiation using Landsat imagery. *GIScience Remote Sens.* **2019**, *56*, 462–484. [[CrossRef](#)]
99. Fu, P.; Rich, P.M. A geometric solar radiation model with applications in agriculture and forestry. *Comput. Electron. Agric.* **2002**, *37*, 25–35. [[CrossRef](#)]
100. Ng, E.; Ren, C. *The Urban Climatic Map: A Methodology for Sustainable Urban Planning*; Routledge: Abingdon, UK, 2015.

101. Conrad, O.; Bechtel, B.; Bock, M.; Dietrich, H.; Fischer, E.; Gerlitz, L.; Wehberg, J.; Wichmann, V.; Böhner, J. System for automated geoscientific analyses (SAGA) v. 2.1. 4. *Geosci. Model Dev.* **2015**, *8*, 1991–2007. [[CrossRef](#)]
102. Badaro-Saliba, N.; Adjizian-Gerard, J.; Zaarour, R.; Najjar, G. LCZ scheme for assessing Urban Heat Island intensity in a complex urban area (Beirut, Lebanon). *Urban Clim.* **2021**, *37*, 100846. [[CrossRef](#)]
103. Estacio, I.; Babaan, J.; Pecson, N.; Blanco, A.; Escoto, J.; Alcantara, C. GIS-based mapping of local climate zones using fuzzy logic and cellular automata. *Int. Arch. Photogramm. Remote Sens. Spat. Inf. Sci.* **2019**, *42*, 199–206. [[CrossRef](#)]
104. Oke, T.R. City size and the urban heat island. *Atmos. Environ.* **1973**, *7*, 769–779. [[CrossRef](#)]
105. Yokobori, T.; Ohta, S. Effect of land cover on air temperatures involved in the development of an intra-urban heat island. *Clim. Res.* **2009**, *39*, 61–73. [[CrossRef](#)]
106. Sun, C.-Y. A street thermal environment study in summer by the mobile transect technique. *Theor. Appl. Climatol.* **2011**, *106*, 433–442. [[CrossRef](#)]
107. Krüger, E.; Givoni, B. Outdoor measurements and temperature comparisons of seven monitoring stations: Preliminary studies in Curitiba, Brazil. *Build. Environ.* **2007**, *42*, 1685–1698. [[CrossRef](#)]
108. Johnson, S.; Ross, Z.; Kheirbek, I.; Ito, K. Characterization of intra-urban spatial variation in observed summer ambient temperature from the New York City Community Air Survey. *Urban Clim.* **2020**, *31*, 100583. [[CrossRef](#)]
109. Ryan, P.H.; LeMasters, G.K. A review of land-use regression models for characterizing intraurban air pollution exposure. *Inhal. Toxicol.* **2007**, *19*, 127–133. [[CrossRef](#)] [[PubMed](#)]
110. Hoek, G.; Beelen, R.; De Hoogh, K.; Vienneau, D.; Gulliver, J.; Fischer, P.; Briggs, D. A review of land-use regression models to assess spatial variation of outdoor air pollution. *Atmos. Environ.* **2008**, *42*, 7561–7578. [[CrossRef](#)]
111. Rosenfeld, A.; Dorman, M.; Schwartz, J.; Novack, V.; Just, A.C.; Kloog, I. Estimating daily minimum, maximum, and mean near surface air temperature using hybrid satellite models across Israel. *Environ. Res.* **2017**, *159*, 297–312. [[CrossRef](#)]
112. Shiflett, S.A.; Liang, L.L.; Crum, S.M.; Feyisa, G.L.; Wang, J.; Jenerette, G.D. Variation in the urban vegetation, surface temperature, air temperature nexus. *Sci. Total Environ.* **2017**, *579*, 495–505. [[CrossRef](#)]
113. Jenerette, G.D.; Miller, G.; Buyantuev, A.; Pataki, D.E.; Gillespie, T.W.; Pincetl, S. Urban vegetation and income segregation in drylands: A synthesis of seven metropolitan regions in the southwestern United States. *Environ. Res. Lett.* **2013**, *8*, 044001. [[CrossRef](#)]
114. Chen, L.; Ng, E.; An, X.; Ren, C.; Lee, M.; Wang, U.; He, Z. Sky view factor analysis of street canyons and its implications for daytime intra-urban air temperature differentials in high-rise, high-density urban areas of Hong Kong: A GIS-based simulation approach. *Int. J. Climatol.* **2012**, *32*, 121–136. [[CrossRef](#)]

Disclaimer/Publisher’s Note: The statements, opinions and data contained in all publications are solely those of the individual author(s) and contributor(s) and not of MDPI and/or the editor(s). MDPI and/or the editor(s) disclaim responsibility for any injury to people or property resulting from any ideas, methods, instructions or products referred to in the content.